J Electroceram (2007) 18:45–55
DOI 10.1007/s10832-007-9007-8

Dielectric relaxation and variable-range-hopping conduction in $BaSn_{1-x}Cr_xO_3$ system

Shail Upadhyay · Om Parkash · Devendra Kumar

Received: 13 May 2005 / Accepted: 8 June 2006 / Published online: 14 March 2007

Abstract The possibility of formation of a solid solution in the system $BaSn_{1-x}Cr_xO_3$ has been explored upto $x \leq 0.20$. It has been confirmed that single phase solid solution forms upto $x \leq 0.10$. Dielectric and conduction behaviour of single phase samples have been studied in the temperature range 400–610 K and frequency range 10 Hz–2 MHz. Two dielectric relaxation processes in two different frequency ranges have been observed. The temperature dependence of both dc and ac resistivity obey relation $\rho = \rho_o \exp(B/T^{1/4})$, indicative of variable range hopping conduction mechanism. The activation energy for dc conduction is higher than that for relaxation time (τ) of low frequency dielectric relaxation process. It has been observed that activation energy for dielectric relaxation matches with activation energy for ac conductivity (at 100 kHz) for both the dielectric relaxation processes. Seebeck coefficient 'α' of the samples have been measured in the temperature range 350–650 K. Negative value of 'α' in the entire range of temperature measurement shows that conduction species are negatively charged. On the basis of value of activation energy for dc conduction and sign of Seebeck coefficient, conduction in the low temperature region (below 500 K) is attributed to hopping of weakly bonded electrons among $Sn^{2+} \Leftrightarrow Sn^{4+}$ or $Sn^{3+} \Leftrightarrow Sn^{4+}$ and that in the high temperature region (above 500 K) to hopping of doubly ionized oxygen vacancies $\left(V_o^{\bullet\bullet}\right)$.

Keywords Perovskite oxide · Barium stannate · Dielectric relaxation · Variable range hopping conduction · Seebeck coefficient

1 Introduction

Barium stannate is a cubic perovskite oxide compound that behaves as a *n*-type semiconductor with a wide band gap of 3.4 eV and is stable at high temperature (upto 1,000 °C). Its high performance application such as semiconductive sensor material for exhaust gases (isobutane, H_2, NO, CO and CH_4) are one of the main reasons for the demand of $BaSnO_3$ perovskite stannate [1–3]. However this perovskite is also interesting for other applications like, thermally stable capacitor due to the characteristics of its dielectric constant. Various methods of synthesis of the barium stannate have been reported [4–8].

The high temperature defect chemistry and mechanism of electrical conduction in perovskite titanates such as $BaTiO_3$ and $SrTiO_3$ are well understood [9–13]. Undoped and nickel doped $SrTiO_3$ have been chosen as model substance, due to their simple cubic structure and availability in ceramic as well as in single crystalline form [14]. Though $BaSnO_3$ is closely related structurally and chemically with well-investigated perovskite compounds $BaTiO_3$ and $SrTiO_3$, the effect of doping and defect chemistry of $BaSnO_3$ have not been studied systematically.

In order to improve the dielectric and sensing behaviour of barium stannate it is worthwhile to study effect of donor

S. Upadhyay (✉)
Department of Applied Physics,
Priyadarshini College of Engineering,
C.R.P.F. Campus, Hingna Road, Nagpur 440 019 M.S., India
e-mail: shail72@yahoo.com

O. Parkash · D. Kumar
Department of Ceramic Engineering, Institute of Technology,
Banaras Hindu University,
Varanasi 221 005 U.P., India

O. Parkash
e-mail: opec_itbhu2003@yahoo.co.in

D. Kumar
e-mail: dkumar_itbhu2003@yahoo.co.in

and acceptor doping on the dielectric and conduction behaviour of the $BaSnO_3$. Only a few reports are available on the effect of doping (La at Ba site and Sb, Ni & Co at Sn site) on electrical conduction behavior of $BaSnO_3$ [14–18]. From the literature survey it is noticed that dopants chosen for Sn site have multiple valence state which complicate the study of effect of acceptor doping on electrical behavior of barium stannate. Therefore in order to study effect of acceptor doping chromium has been chosen as dopant for Sn site in $BaSnO_3$ because chromium mostly exists in Cr^{3+} ion state. In this paper, dielectric and conduction behaviour of $BaSn_{1-x}Cr_xO_3$ system is reported. To the best of authors knowledge the samples in the system $BaSn_{1-x}Cr_xO_3$ have not been synthesized and characterized so far. This will be first report on this system.

2 Experimental procedure

Samples with compositions x=0.00, 0.01, 0.05, 0.10, 0.15 and 0.20, in the chromium doped barium stannate system, $BaSn_{1-x}Cr_xO_3$ were prepared by solid state reaction method. The various compositions have been referred throughout this paper by abbreviated name BSC0 (for x=0.00), BSC1 (for x=0.01), BSC5 (for x=0.05), BSC10 (for x=0.10), BSC15 (for x=0.15) and BSC20 (for x=0.20). The Details of processing procedure is reported elsewhere [19].

For microstructural characterization, freshly fractured surfaces of the sintered pellets were coated with Au–Pd alloy by sputtering method using sputtering unit (CIKO-8000, Japan). Scanning electron micrographs were recorded at different magnifications with the help of a scanning electron microscope (Jeol JSM 840 A). For determination of single phase solid solution formation, X-ray diffraction (XRD) patterns of the powder of finally sintered pellets were recorded with diffractometer (Rigaku Rotoflux RTC-300) employing $CuK\alpha_1$ radiation.

For electrical and dielectric measurements sintered pellets were polished and washed with isopropanol to remove adsorbed moisture. These pellets were electroded using Ag–Pd paint (Elteck) by maturing at 1,075 K for 20 min. In order to avoid interference from effect of humidity, whole assembly was heated upto temperature 650 K and during cooling, capacitance (C), dissipation factor (D) and conductance (G) of single phase samples BSC0, BSC1, BSC5 and BSC10 (with x=0.00, 0.01, 0.05 and 0.10) were measured using Hewlett Packard-4192 A LF impedance analyzer, as a function of frequency (10 Hz–2 MHz) in the temperature range 400–610 K.

Seebeck coefficient 'α' of the samples were measured in the temperature range 350–650 K by the differential method. Seebeck coefficient 'α' was measured by pressing a thick (5–7 mm) pellet of the samples between two spring loaded platinum foils in an indigenously fabricated sample holder. An auxiliary heater is placed around one of the surface of the pellet to get a temperature gradient of 5–10 °C across the sample. The temperature gradient was measured with the help of two platinum—rhodium thermo-couple which were kept very close to the sample, while thermo-e.m.f was measured with the help of digital micro-voltmeter with an accuracy of ±3%. Seebeck coefficient 'α' of the samples were calculated using relation $\alpha = -(\Delta V/\Delta T)$ where ΔV and ΔT are the voltage and temperature difference measured across the sample, respectively. In this formulation the potential at higher temperature is taken positive.

3 Results and discussions

3.1 Crystal structure and microstructure

X-ray diffraction (XRD) patterns of the samples BSC0, BSC1, BSC5 and BSC10 revealed the formation of single-phase solid solution. Formation of single phase was confirmed on the basis of absence of characteristic lines of the constituent oxides or other phases present if any in the system, in the powder X-ray diffraction (XRD) patterns. Thus the solubility of chromium in barium stannate is limited upto $x \leq 10$ at.%. The XRD patterns of the other samples i.e. BSC15 and BSC20, show extra lines due to

Table 1 Lattice parameter and activation energy for dc conduction of the samples in the $BaSn_{1-x}Cr_xO_3$ system.

Composition (x)	Sample code	Lattice parameter (Å)	Grain size (μm)	Temperature region (K)	Activation energy (eV)
0.00	BSC0	4.123±0.001	2–4	400–500	0.11±0.01
				500–610	0.54±0.01
0.01	BSC1	4.121±0.002	2–4	400–500	0.12±0.01
				500–610	0.96±0.02
0.05	BSC5	4.119±0.001	1–2	400–500	0.12±0.01
				500–610	0.92±0.01
0.10	BSC10	4.116±0.001	1–2	400–500	0.10±0.02
				500–610	0.87±0.01

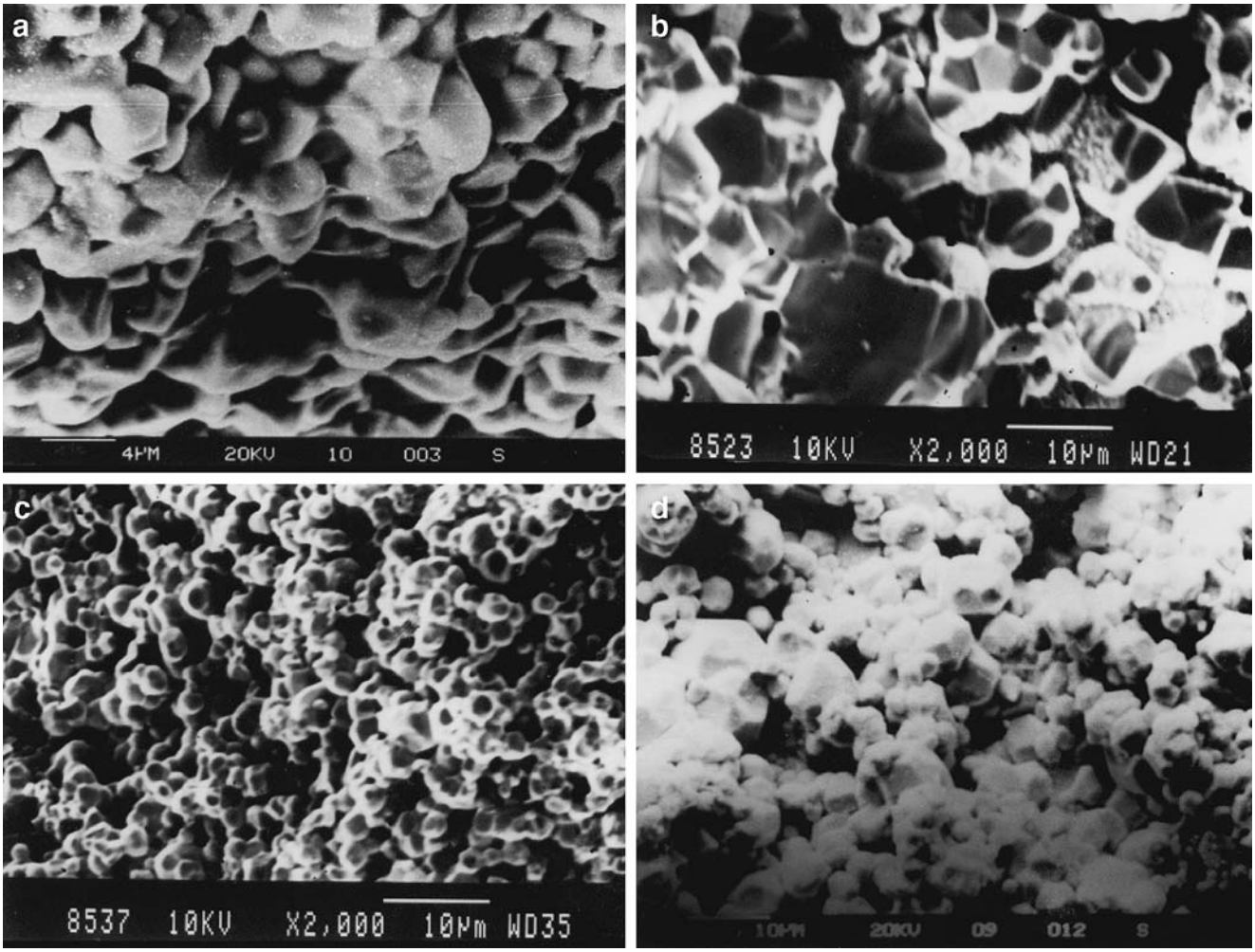

Fig. 1 Scanning electron micrograph (SEM) of fractured surfaces of sample **a** BSC0, **b** BSC1, **c** BSC5 and **d** BSC10

reflection from the planes of constituents oxide (chromium and tin oxides). The XRD data of single phase compositions is indexed on the basis of cubic unit cell similar to undoped $BaSnO_3$ reported in the literature [20]. The value of lattice parameter for all the single phase compositions is given in Table 1. It is observed that lattice parameter decreases with increasing x. This is due to replacement of Sn^{4+} ions (0.69 Å) by Cr^{3+} ions with a small radii (0.62 Å).

Scanning electron micrographs (SEM) of freshly fractured surfaces for the samples BSC0, BSC1, BSC5 and BSC10 are shown in Fig. 1. The grain size of the BSC1 is same as that of BSC0 but of other samples i.e BSC5 and BSC10 is smaller. The acceptors are reported to be grain growth inhibitors in alkaline earth titanates [21]. The small grain size of BSC5 and BSC10 samples is attributed to segregation of acceptors at grain boundaries.

3.2 Dielectric behaviour

In the system $BaSn_{1-x}Cr_xO_3$ it has been observed that nature of variation of dielectric constant, dissipation factor and ac conductivity with temperature and frequency remain same for all samples i.e. for BSC0, BSC1, BSC5 and BSC10, therefore we have chosen BSC5 sample as a representative of the whole system $BaSn_{1-x}Cr_xO_3$, and figures are displayed for this sample only.

Variation of dielectric constant, ε_r and dissipation factor, D for sample BSC5, with temperature at three frequencies 1, 10 and 100 kHz are shown in Fig. 2a and b, respectively. It is noticed from Fig. 2 that both dielectric and dissipation factor remain constant upto 500 K at all the frequencies, thereafter both increases rapidly. The rate of increase of dielectric constant with temperature decreases with increasing frequency. The sharp increase of ε_r with temperature at 1 kHz may be due to interfacial polarization.

The variation of ε_r and D with frequency at temperatures 400 and 610 K are shown in Fig. 3a and b, respectively. It is observed that in the low frequency range (10 Hz–1 kHz), strong dispersion is observed in ε_r, after that it remains almost independent of frequency upto 10 kHz, thereafter it decreases linearly with increasing frequency. D also decreases (in low frequency range) in the same manner

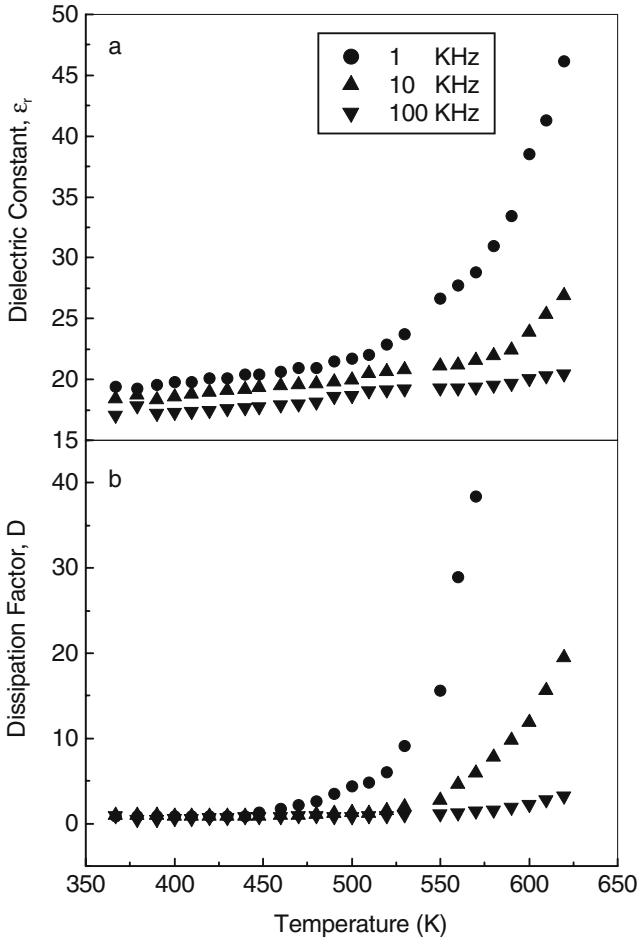

Fig. 2 Variation of **a** relative dielectric constant, and **b** dissipation factor with temperature for sample BSC5

as ε_r decreases but in this plot a hump is observed above 1 kHz. Further, it is observed that as temperature increases, position of hump shifts towards higher frequency side and at the highest temperature of measurements (610 K) its position become out of our instrument measuring frequency range (above 2 MHz). It is also noticed that with increasing temperature, low frequency dispersion become more pronounced. From these plots it is obvious that dielectric behaviour of these materials is composed of two components. The low frequency dispersion lies well within the frequency range for relaxation of space charge polarization (1 Hz–1 kHz), whereas hump lies in the relaxation range of dipolar polarization (1 kHz–1 MHz). Thus dielectric loss of these materials is resultant of two kind of polarizations, space charge (low frequency) and dipolar (high frequency) polarization. Low frequency loss (dispersion in ε_r and D) may be due to dc conduction or relaxation of space charge polarization. Interfacial polarization (space charge) polarization arises whenever phases with different conductivities are present. As these materials have been synthesized by a slow diffusion controlled thermochemical process due to which random occupation of equivalent sites by different ions takes place, which leads to the possibility of existence of microheterogeneities in the end products. In the present case, octahedral sites are occupied randomly by Sn^{4+}, Sn^{2+}, Sn^{3+} and Cr^{3+} ions. Because of these chemical microheterogeneities, samples have different microregions with varying conductivity. These microregions give rise to interfacial polarization. The interfacial polarization may arise due to presence of grain boundaries, if grain boundaries have different conductivity than that of grains.

These materials were synthesized by solid state ceramic method at 1,650 K. At this temperature there is a possibility that oxygen leave the lattice according to equation:

$$O_O \rightarrow 1/2\,O_2 + V_O^{\bullet\bullet} + 2e' \quad (1)$$

These materials have one element Sn which is a multivalent ion, therefore, electrons released in the process given by Eq. 1 may be captured by Sn^{4+} to produce Sn^{2+} and Sn^{3+}. From the ESR studies of these materials it has been confirmed that other elements (Ba and Cr) remain in 2+ and 3+ oxidation state, respectively. Sn^{2+} and Sn^{3+} ions at Sn^{4+} will considered as negatively charged defects such as $\left(Sn^{2+}{}_{Sn}{}^{4+}\right)''$ and $\left(Sn^{3+}{}_{Sn}{}^{4+}\right)'$. In general substitution of

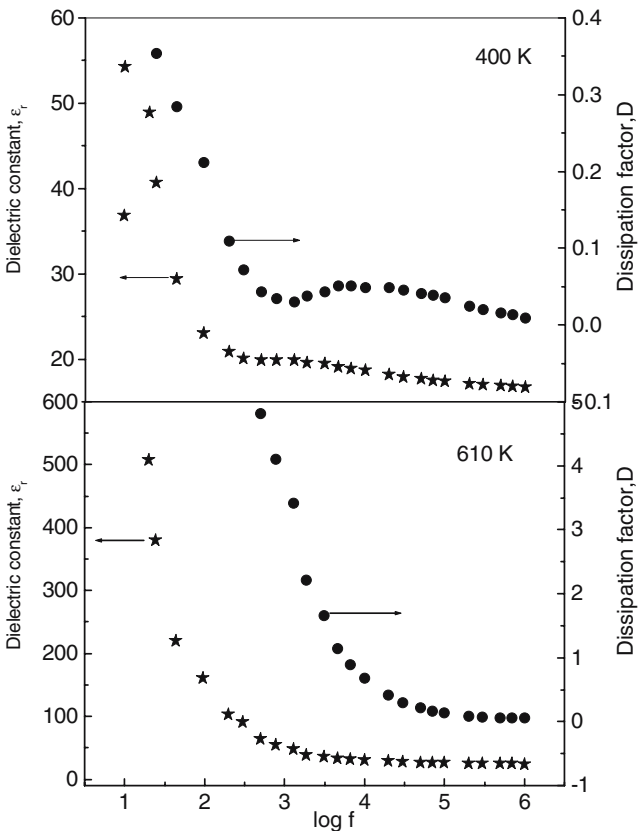

Fig. 3 Variation of dielectric constant and dissipation factor with frequency for sample BSC5

acceptor (M) at B site of perovskite oxide, ABO_3, electrical charge neutrality is maintained either by creation of oxygen vacancies or holes which depends on the level of doping. Equations for charge compensation mechanism are given below:

$$M_2O_3 \xrightarrow{ABO3} 2M_B'' + V_O^{\bullet\bullet} + 3\,O_O \quad (2)$$

$$1/2\,O_2 + M_2O_3 \xrightarrow{ABO3} 2M_B'' + 2h^{\bullet} + 4O_O \quad (3)$$

Low value of dielectric constant and dissipation factor of these materials indicate that charge compensation is mainly taking place due to creation of oxygen vacancies (according to Eq. 2) in the samples. Many experimental findings give strong indication that in undoped and acceptor doped $BaTiO_3$ and $SrTiO_3$ ceramics, oxygen vacancies are predominantly doubly ionized at all the temperatures [14]. At low temperatures, association between negatively charged acceptors and oxygen vacancies form dipoles namely $\left[\left(Sn^{2+}{}_{Sn}{}^{4+}\right)'' - V_O^{\bullet\bullet}\right]$ or $\left[\left(Sn^{3+}{}_{Sn}{}^{4+}\right)' - V_O^{\bullet\bullet} - \left(Sn^{3+}{}_{Sn}{}^{4+}\right)'\right]$ or $\left[\left(Cr^{3+}{}_{Sn}{}^{4+}\right)' - V_O^{\bullet\bullet} - \left(Cr^{3+}{}_{Sn}{}^{4+}\right)'\right]$. These dipoles can change their orientation owing to jumping of oxygen ions into vacant oxygen site of oxygen octahedron or due to hopping of electrons among Sn^{2+} and Sn^{4+} or Sn^{3+} and Sn^{4+} bound to oxygen vacancies.

Variation of imaginary part of permittivity (ε'') with real part of permittivity (ε') i.e Cole–Cole plot for sample BSC5, at three temperatures of interest are shown in Fig. 4. It is observed that two depressed arcs are present but low frequency arc is much larger compared to high frequency arc. Due to limitation of our measuring temperature and frequency ranges, complete portion of low frequency arc is not seen, therefore, it is not possible to obtained relaxation time and its variation with temperature for the low frequency dielectric relaxation process.

In many dielectrics, a dc conductivity related dielectric relaxation is observed at low frequencies [22, 23]. In ionic conductors such as glasses, this conductivity related dielectric relaxation is often called the migration loss [24]. In evaluation of the low frequency dielectric relaxation of these materials, it is customary to subtract the dc conductivity contribution from the dielectric loss. Due to this subtraction procedure, it is often difficult to obtain an accurate value of the permittivity at low frequency. Thus alternate quantities such as admittance, impedance and electric modulus are used without subtraction of the dc conductivity contribution to evaluate low frequency dielectric characterization [25–27]. Since these quantities are related to the permittivity, therefore we have used complex plane impedance and electric modulus analysis to study low frequency dielectric characteristics of these samples.

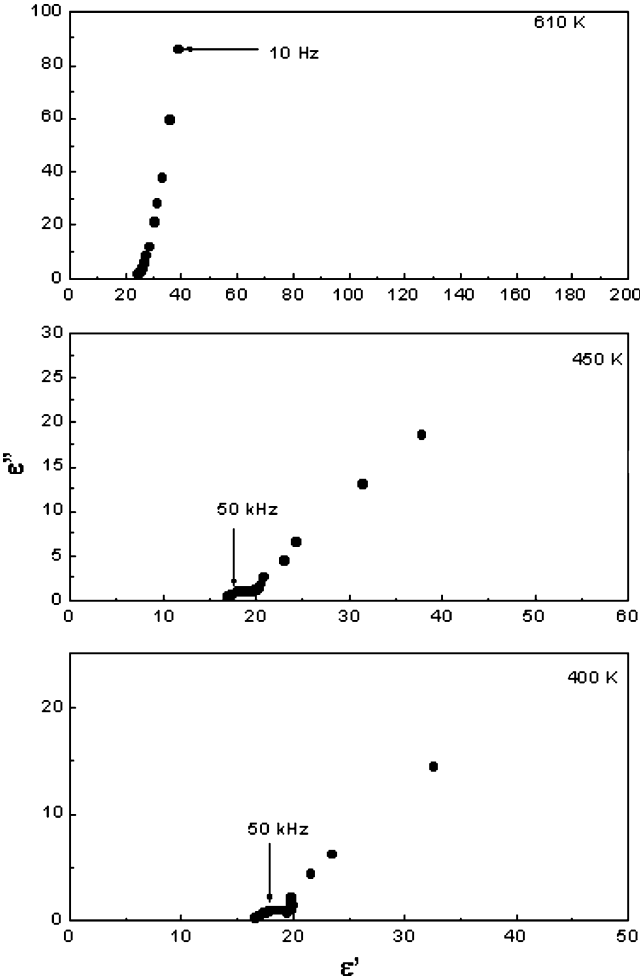

Fig. 4 Cole–Cole plots for permittivity at three different temperatures for sample BSC5

3.3 Complex plane impedance and modulus spectroscopy

Typical complex plane impedance plot (Z'' vs Z') at three different temperatures for BSC5 are shown in Fig. 5. At low temperature (400 K), materials exhibit strong insulating behaviour and in complex plane impedance plot, a line almost parallel to Z'' axis is observed. As temperature increases shape of the impedance spectra changes for example at 450 and 500 K, single slightly depressed semicircle is seen and on further increase in temperature (at 550 and 610 K) two poorly resolved semicircles are observed. These observations suggest that below 500 K relaxation time for grains and grain boundaries is same but as the temperature increases their relaxation time differs. In the complex plane impedance plot, the intercept of the single semicircular arc with Z' axis represents the bulk dc resistance of the sample and the value of bulk capacitance can be obtained by using relation $2\pi f_{max}RC=1$ (where f_{max}= frequency at the apex of the arc). Bulk dc conductivity of the sample was calculated using relation : $\sigma=1/R_b(d/A)$

where A—cross section area of the sample and d—thickness of the sample. Generally contribution of electrode-sample interface to total resistance of a polycrystalline ceramic sample is small. If total resistance of the sample is sufficiently high this electrode-sample contribution can not be observed in the impedance plots, therefore for these samples electrode-sample contribution to the total resistance is neglected. At high temperature, low frequency arc is assigned to grain boundaries whereas high frequency to the grains. The resistance and capacitance value of grains and grain boundaries at 610 K have been obtained by manual fitting of impedance data. These values are given below:

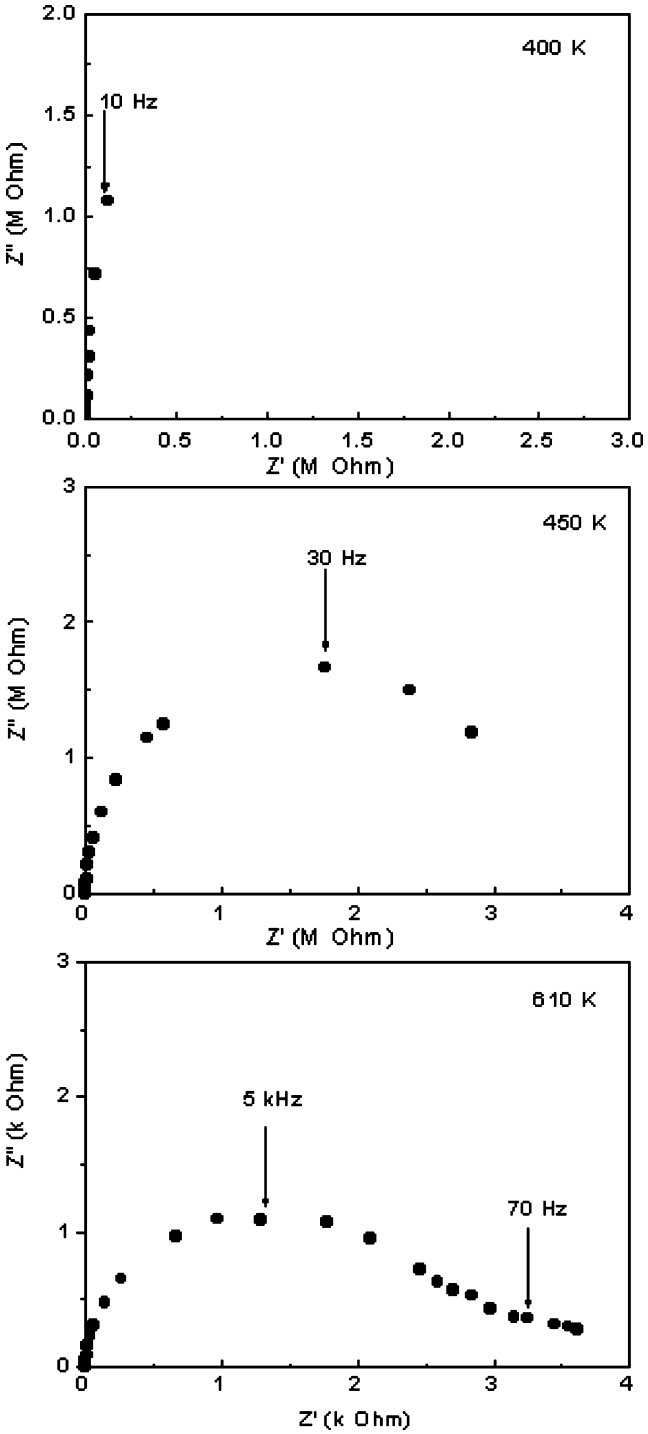

Fig. 5 Complex plane impedance plots at three different temperatures for sample BSC5

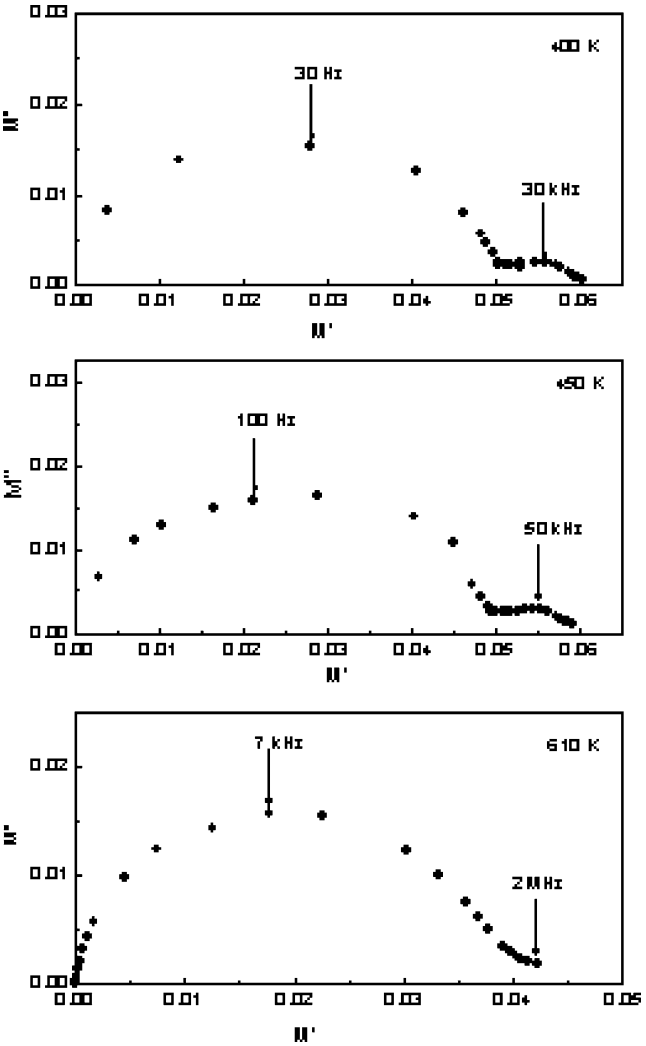

Fig. 6 Complex plane modulus plots at three different temperatures for sample BSC5

$R_g=2.65\times10^6$ Ohm	$C_g=1.5\times10^{-11}$ F
$R_{gb}=9.95\times10^5$ Ohm	$C_{gb}=1.4\times10^{-9}$ F

It is not possible to delineate the contribution of grains and grain boundaries at all the temperatures of measurement using complex plane impedance plot, hence the same data have been replotted in the complex plane modulus plots (M″ vs M′ plot). These plots for BSC5 sample are shown in Fig. 6. Two slightly depressed arcs have been observed. It is observed that total intercept of the arcs on M′ axis does not change much with temperature. The position of maxima of the arcs shifts

towards higher frequency side with increasing temperature. The intercept of the arc on the real (M′) axis is given as C_0/C (where $C_0=A/d$ and C—capacitance of the corresponding contribution i.e grains or grain boundaries). If low frequency arc represents grain boundaries contribution and high frequency arc to the grains then from the intercept of the arcs, one can conclude that capacitance value of grains is high as compared to that of grain boundaries, which is contradictory to general observation that capacitance value of grains is much lower than that of the grain boundaries. From the analysis of the equivalent circuit for a polycrystalline ceramic ionic conductors, it has been shown that M″ vs M′ plots reflect the bulk properties, since M″ is inversely proportional to the capacitance of the circuit element, and grain boundaries capacitance is number of orders of magnitude higher than that of the grains [28]. Modulus plots highlight dielectric relaxation process of materials (because $M^*=1/\varepsilon_o\omega\varepsilon^*$), thus one can say that these two semicircles corresponds to two dielectric relaxation processes which are observed in bulk behaviour of the sample BSC5.

The low frequency arc is assigned to relaxation of space charge polarization and high frequency to the dipolar polarization. Relaxation time, τ, for both the processes was determined from the peak position of the corresponding semicircular arc at different temperatures. Log τ have been plotted as a function of inverse of temperature and is shown in Fig. 7. Both the relaxation processes follow an Arrhenius relationship given below:

$$\tau = \tau_o \exp\left(E_{\text{relax.}}/k_B T\right) \quad (4)$$

where τ_o is the relaxation time at infinite temperature, E_{relax} the activation energy for relaxation, k_B Boltzmann's constant and T the absolute temperature. From the least square fitting of the data, activation energy for the both the relaxation processes were obtained. The activation energy for low and high frequency dielectric relaxation processes is found to be 0.53±0.02 and 0.11±0.03 eV, respectively. The value of τ_o for low and high frequency relaxation processes is found to be 10^{-8} and 9×10^{-7} s, respectively. If low frequency relaxation is due to dc conduction then activation energy for dc conduction and relaxation time of low frequency dielectric relaxation process should be almost equal. In order to check the above mentioned possibility, electrical conduction behaviour of these samples have been studied.

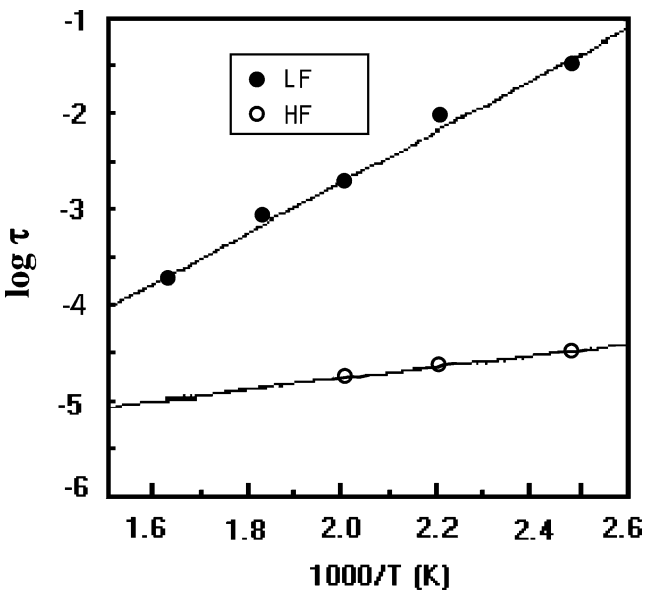

Fig. 7 Variation of low and high frequency relaxation time with inverse of temperature for sample BSC5

3.4 Electrical conduction

Plots of log σ_{ac} with log f at a few temperatures for BSC5 sample is shown in Fig. 8. It is observed that σ_{ac} remains independent of frequency upto certain frequency, thereafter it increases linearly with frequency. The frequency independent region increases with increasing temperature. It has been confirmed that bulk dc conductivity calculated from resistance value obtained from the intercept of single semicircular arc in Z″ vs Z′ plots (Fig. 5) matches with conductivity obtained from intercept of low frequency plateau of log σ_{ac} vs log f plot, therefore ac conductivity at 10 Hz frequency is considered as dc conductivity. The variation of log σ_{dc} with concentration of chromium in the system $BaSn_{1-x}Cr_xO_3$ at 400 K is shown in Fig. 9. It is observed that resistivity of the samples BSC1, BSC5 and BSC10 is high as compared to the sample BSC0. It is reported that barium stannate is a n-type semiconductor in its usual fired state because of the presence of small amount of Sn^{2+} and Sn^{3+} due to loss of oxygen during firing [2]. Addition of a cation of lower valance (acceptor) such as Cr^{3+} at Sn^{4+} reduces the number of electrons (and it encourages the Sn^{4+} to have 4+valence), which raises resistivity. The linear increase of conductivity from BSC1 to BSC10 may be due to increase in number of oxygen vacancies as the amount of cation increases.

Plot of log σ_{ac} with inverse of temperature (1,000/T) at frequencies 10 Hz (dc), 1 kHz,10 kHz and 100 kHz are shown in Fig. 10, for sample BSC5. Two regions are observed in these plots : (a) a low temperature region where slope is small and strong frequency dependence (400–500 K), and (b) a high temperature region with higher slope and low frequency dependence (500–610 K). The activation energy for dc conductivity in both the temperature regions for all the samples were obtained from the least square fitting of the data according to Arrehenius relationship

$$\sigma = \sigma_o \exp\left(-E_a/kT\right) \quad (5)$$

and value of activation energy is given in Table 1. From the table it is noticed that the activation energy in the low and

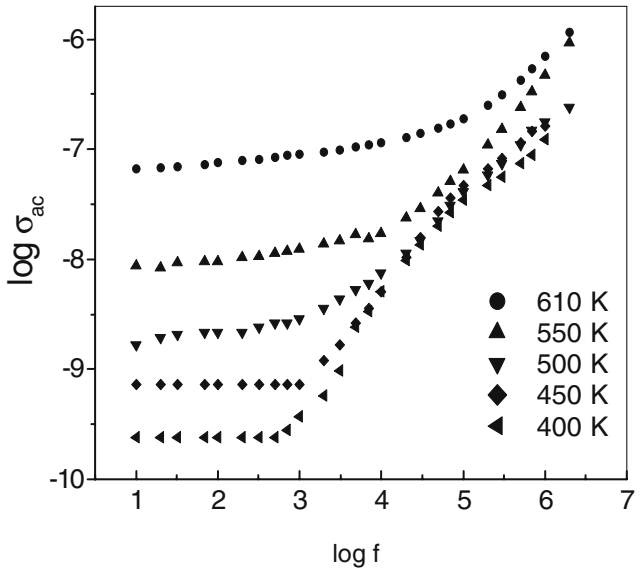

Fig. 8 Variation of logarithm of AC conductivity with logarithm of frequency for sample BSC5

high temperature regions for BSC5 sample is 0.12±0.02 and 0.92±0.01 eV, respectively. It is observed that activation energy in the low temperature range is almost equal for all the samples (i.e. BSC0, BSC1, BSC5 and BSC10) but in the high temperature region it varies with conductivity of the samples. The activation energy in the high temperature range is highest for sample BSC1 and lowest for sample BSC0. Moreover, it has been observed that low temperature range (400–500 K) and corresponding activation energy (~ 0.11 eV) is same for other perovskite stannates based samples investigated in our laboratory [18, 29–31].

The activation energy for ac conductivity (for σ_{ac} at 100 kHz) is 0.10±0.01 and 0.55±0.02 eV, respectively in

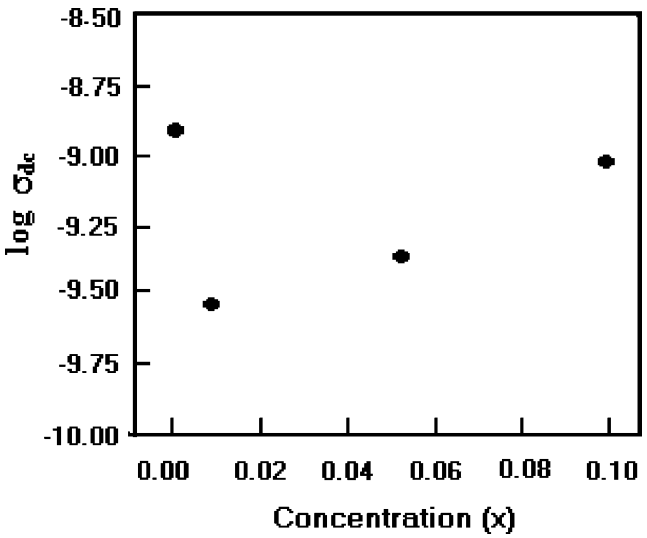

Fig. 9 Variation of dc conductivity at 400 K with concentration of dopant in the system $BaSn_{1-x}Cr_xO_3$

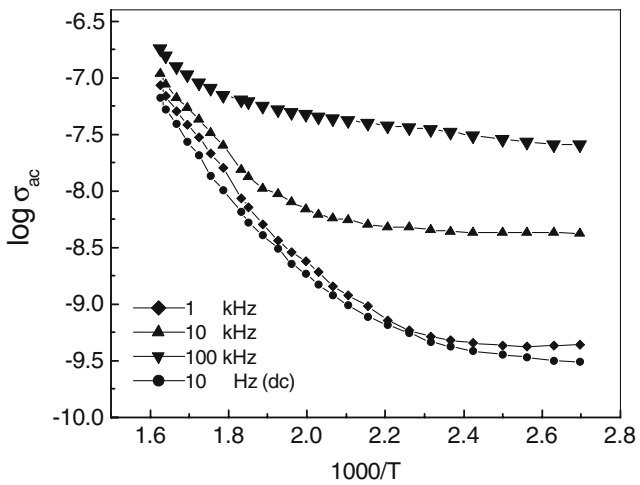

Fig. 10 Variation of logarithm of AC conductivity with inverse of temperature for sample BSC5

low and high temperature regions for sample BSC5. It is observed that activation energies for ac conductivity at 100 kHz in low and high temperature regions matches with the activation energy of relaxation time of high and low frequency dielectric relaxation processes (Fig. 7).

A large numbers of disordered solids show a frequency dependent conductivity in the frequency range 1 to 10^6 Hz [32]. Their conductivity as a function of frequency is given by

$$\sigma(\omega) = \sigma_o + \sigma_1(\omega) \tag{6}$$

where σ_o is dc conductivity and σ_1 is ac conductivity which is given as $\sigma_{ac}=\omega^s$ where $0 \le s \le 1$. Exponent, 's' is both frequency and temperature dependent parameter. For the samples in the system $BaSn_{1-x}Cr_xO_3$, 's' decreases with increasing temperature. The most common explanation for a conductivity which increases with frequency is the existence of one or the other kind of inhomogeneities. The general features of ac conduction in disordered solids which are observed almost without exception are following [33] : (1) for $\sigma(\omega)$ one observes at high frequencies an approximate power law with an exponent 's' less than or equal to one. (2) At lower frequencies there is gradual transition to a frequency independent conductivity. (3) Whenever the dc conductivity is measurable there is always a dielectric loss peak. (4) The temperature dependence of σ_o and ω_m (dielectric loss peak frequency) are usually of Arrhenius type with the same activation energy. (5)The shape of the dielectric loss peak is temperature independent. (6) The ac conductivity is much less temperature dependent than the dc conductivity. For 's' very close to one, the ac conductivity is practically independent of temperature. (7) The exponent 's' decreases with increasing temperature and as T→0,s→1. Thus ac conductivity becomes almost temperature independent. (8) Even though σ_o may vary many orders of magnitude the ac conductivity varies relatively little for different solids and different temperatures.

Various models have been proposed for conduction behaviour of disordered solids among them is hopping model [34]. In this model one assume the presence of inhomogeneity on the atomic scale, by assuming randomly varying jump frequencies for charge carriers [33]. The model is based on the assumption of existence of randomly varying free-energy barriers for jump of charge carriers. Variable-range-hopping mechanism has been obtained in some amorphous materials via "states in the energy gap" which have been attributed to the di-vacancies and dangling bonds. In other words, it comes from some type of lattice disorder [35].

Frequency and temperature dependence of conductivity of the samples BSC0, BSC1, BSC5 and BSC10 satisfies almost all the general features exhibited by disordered materials mentioned above. The presence of different kinds of ions at Sn sites of $BaSnO_3$ lattice may result in localized distortion due to random occupation of equivalent sites by different heterovalent ions, which further leads to fluctuation in the structure giving rise to distortion. As mentioned in Section 3.2 of this paper that defects $\left(Sn^{2+}_{Sn}{}^{4+}\right)''$, $V_O^{\bullet\bullet}, V_O^{\bullet}, \left(Sn^{3+}_{Sn}{}^{4+}\right)'$ and $\left(Cr^{3+}_{Sn}{}^{4+}\right)'$ are randomly distributed in space and energy which may be responsible for disorder in these samples. Therefore in these samples conduction may occur via variable-range-hopping of charge carriers. For variable-range-hopping conduction mechanism, resistivity should obey relation given below [36]

$$\rho = \rho_o \exp\left(B/T^{1/4}\right) \tag{7}$$

where $B = \left[(\lambda\alpha^3)/(k_B N(E_F)\right]^{1/4}$ where λ—a dimensionless constant, α—localization length, $N(E_F)$—density of state at Fermi level and k_B—Boltzman's constant. Plot of ln (ρ) vs $T^{-1/4}$ for both ac (at 100 kHz) and dc conduction in temperature region 500–610 K for sample BSC5 are shown in Fig. 11. The linearity of the plots show that conduction in these materials is taking place via variable range hopping mechanism. In order to cross check the variable-range-hopping mechanism, ln [ln(ρ/ρ_o)] is plotted against ln T for both dc and ac resistivety and shown in Fig. 12. An average slope equal to 1/4 confirmed variable-range-hopping conduction mechanism for both dc and ac processes. Based on

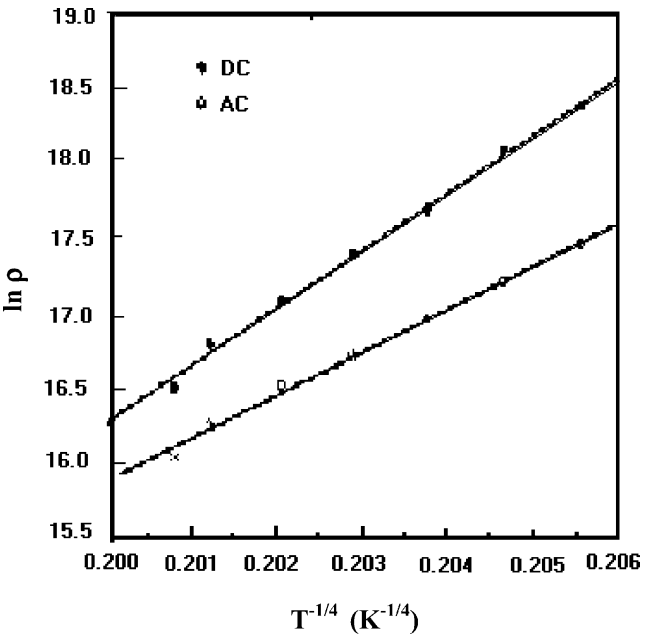

Fig. 11 Variation of logarithm of DC and AC resistivity with $T^{-1/4}$ for sample BSC5

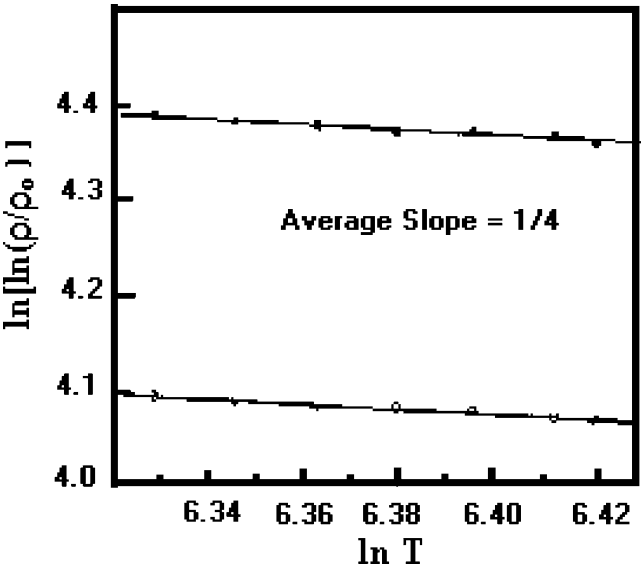

Fig. 12 Variation of logarithm of logarithm resistivity with logarithm of temperature for sample BSC5

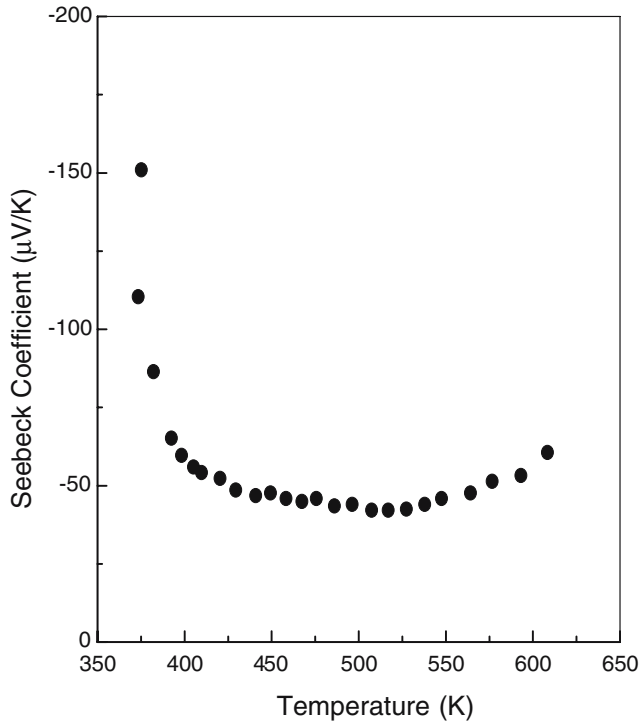

Fig. 13 Variation of Seebeck coefficient with temperature for sample BSC5

dielectric and ac conductivity studies following explanations are proposed for conduction and dielectric relaxation: These materials have dipoles namely $\left[\left(Sn^{2+}{}_{Sn}{}^{4+}\right)'' - V_O^{\bullet\bullet}\right]$ or $\left[\left(Sn^{3+}{}_{Sn}{}^{4+}\right)' - V_O^{\bullet\bullet} - \left(Sn^{3+}{}_{Sn}{}^{4+}\right)'\right]$ or $\left[\left(Cr^{3+}{}_{Sn}{}^{4+}\right)' - V_O^{\bullet\bullet} - \left(Cr^{3+}{}_{Sn}{}^{4+}\right)'\right]$ These dipoles can change their orientation in two ways (1) due to hopping of electrons among $Sn^{2+} \Leftrightarrow Sn^{4+}$ or $Sn^{3+} \Leftrightarrow Sn^{4+}$, and (2) due to hopping of $V_O^{\bullet\bullet}$ within oxygen octahedron. In the low temperature region (below 500 K), low activation energy (~0.11 eV) indicates that reorientation of dipoles is taking place by hopping of electrons. In the high temperature region (above 500 K) due to hopping of oxygen vacancies, $V_O^{\bullet\bullet}$. The observed activation energies for low and high temperature regions are in agreement with activation energy reported for hopping of electrons and $V_O^{\bullet\bullet}$ in other perovskite oxides [18, 29, 34, 37–39].

In the acceptor doped $BaTiO_3$ and $SrTiO_3$ systems, conduction is mainly due hopping of p-type small polaron among acceptor sites. Though $BaSnO_3$ is structurally similar to $BaTiO_3$ and $SrTiO_3$ but conduction mechanism for acceptor doped $BaSnO_3$ may be different due to presence of multivalent Sn element. To support the conduction mechanism (hopping of electrons among Sn^{3+} or Sn^{2+} and Sn^{4+} sites) mentioned above, Seebeck coefficient 'α' of the samples have been measured in the temperature range 350–650 K. The variation of 'α' with temperature for sample BSC5 is shown in Fig. 13. It is clear from the Fig. 13 that magnitude of 'α' decreases sharply upto 400 K after that it becomes almost constant upto 500 K and thereafter start increasing slowly. Similar variation is observed for other samples also but absolute value of 'α' is different for different samples. The common feature for all the samples is 'α'is found to be is negative over entire range of temperature measurement. The negative sign of Seebeck coefficient is an indication that negatively charged ions are responsible for conduction in the entire range of temperature measurements. Negative sign of Seebeck coefficient below 500 K shows that even on Cr^{3+} doping at Sn^{4+} site in $BaSnO_3$, few Sn^{2+} or Sn^{3+} ions are present and conduction is taking place by hopping of electrons among Sn^{2+} to Sn^{3+} or Sn^{3+} to Sn^{4+} ions. Conduction above 500 K is attribution to thermal diffusion of doubly ionized oxygen $\left(V_O^{\bullet\bullet}\right)$ vacancies.

4 Conclusions

Solubility of chromium in the present system is upto $x \leq 10$ at.%. Limited solubility is attributed to substitution of heterovalent ion Cr^{3+} at Sn^{4+} sites in $BaSnO_3$ lattice. Lattice parameter and grain size decreases with increasing chromium concentration. In the measured frequency (10 Hz–2 MHz) and temperature (400–610 K) ranges, two dielectric relaxation and conduction processes are taking place. Seebeck coefficient 'α' of the samples is found to be negative in the entire range of temperature measurement. On the basis of the results of dc conductivity and Seebeck coefficient measurements it is concluded that in the low temperature region (400–500 K) conduction is taking place by variable-range-hopping of electrons among $Sn^{2+} \Leftrightarrow Sn^{4+}$ or $Sn^{3+} \Leftrightarrow Sn^{4+}$. In the high temperature region (500–610 K) due to variable-range-hopping of doubly ionized oxygen vacancies, $V_O^{\bullet\bullet}$.

Acknowledgements Authors are grateful to the Department of Science and Technology (DST) and University Grant Commission (UGC), Government of India, New Delhi for financial assistance.

References

1. J. Cerda, J. Arbiol, R. Diaz, G. Dezanneau, J.R. Morie, Mater. Lett. **56**, 131 (2002)
2. Y. Shimizu, Y. Fukuyama, T. Narikio, H. Arai, T. Seiyama, Chem. Lett. **377**, (1985)
3. B. Ostrick, M. Fleischer, U. Lampe, H. Meixner, Sens. Actuators B **44**, 601 (1997)
4. A.M. Azad, M. Hashim, S. Bapist, A. Badri, A.U. Haq, J. Mater. Sci. **35**, 5475 (2000)
5. S.Y. Jung, K. Seungwan, J. Ind. Eng. Chem. **7**, 183 (2001)
6. S. Upadhyay, O. Parkash, D. Kumar, J. Mater. Sci. Lett. **16**, 1330 (1997)
7. A.M. Azad, L.L.W. Shyna, T.Y. Pang, C.H. Nee, Ceram. Int. **26**, 685 (2000)
8. C.P. Udawatte, M. Kakihana, M. Yoshimura, Solid State Ion. **108**, 23 (1998)
9. L.C. Walter, R.E. Grace, J. Phys. Chem. Solids **28**, 239 (1967)
10. N.H. Chan, D.M. Smyth, J. Electrochem. Soc. **123**, 1584 (1976)
11. J. Daniels, K.H. Hardtl, D. Hennings, R. Wernicke, Philips Res. Rep. **31**, 489 (1976)
12. H.J. Hagemann, D. Hennings, J. Am. Cerm. Soc. **64**, 590 (1981)
13. N.H. Chan, R. K. Sharma, D.M. Smyth, J. Electrochem. Soc. **128**, 1762 (1981)
14. R. Waser, J. Am. Cerm. Soc. **74**, 1934 (1991)
15. S. Upadhyay, Om Parkash, D. Kumar, J. Phys. D: Appl. Phys. **37**, 1483 (2004)
16. M. Lichernan, A. Blin, Int. J. Inorg. Mater. **2**, 281 (2000)
17. Om Parkash, D. Kumar, K.K. Srivastava, R.K. Dwivedi, J. Mater. Sci. **36**, 5805 (2001)
18. Shail Upadhay, Ph.D. thesis, Banaras Hindu University, Varanasi, India, 1998
19. S. Upadhyay, O. Parkash, D. Kumar, Mater. Lett. **49**, 251 (2001)
20. A.J. Smith, J.E. Welch, Acta Crystallogr. **13**, 653 (1960)
21. D.A. Chang, T.Y. Tseng, Mater. Lett. **9**, 943 (1990)
22. M. Tomozawa, *Treatise on Materials Science and Technology, vol. 12*, (Academic Press, London, 1977), p. 283
23. A.E. Owen, Prog. Ceram. Sci. **3**, 77 (1963)
24. F.A. Grant, I.M. Hodge, M.D. Ingram, A.R. West, J. Am. Ceram. Soc. **60**, 226 (1977)
25. F. A. Grant, J. Appl. Phys. **29**, 76 (1987)
26. D. Ravaine, J.P. Diard, J.L. Souquet, J. Chem. Soc., Faraday Trans. II **71**, 1935 (1975)
27. P.B. Macedo, C.T. Moyaihan, R. Bose, Phys. Chem. Glasses **13**, 171 (1972)
28. P. Sarkar, P.S. Nicholson, J. Am. Ceram. Soc. **72**, 1483 (1989)

29. O. Parkash, K.D. Mandal, C.C. Christopher, M.S. Sastry, D. Kumar, J. Mater. Sci. **31**, 4705 (1996)
30. O. Parkash, K.D. Mandal, C.C. Christopher, M.S. Sastry, D. Kumar, Bull. Mater. Sci. **17**, 4705 (1994)
31. O. Parkash, K.D. Mandal, M.S. Sastry, J. Alloys Compd. **228**, 177 (1995)
32. A.R. Long, Adv. Phys. **31**, 553 (1982)
33. J.C. Dyre, J. Appl. Phys. **64**, 2456 (1988)
34. R. Stumpe, Phys. Status Solidi A **88**, 315 (1985)
35. N.F. Mott, E.A. Davis, *Electronic Processes in Noncrystalline Materials*, 2nd edn. (Clarendon, Oxford, 1979)
36. C. Ang, J.R. Jurado, Z. Yu, M.T. Colomer, J.R. Frade, J.H. Baptista, Phys. Rev. B **57**, 11858 (1998)
37. W.L. Warren, K. Vanheusdem, D. Dimos, G.B. Pike, B.A. Tuttle, J. Am. Ceram. Soc. **79**, 536 (1996)
38. M. Vollmann, R. Hugenbeck, R. Waser, J. Am. Ceram. Soc. **80**, 2301 (1997)
39. J.C.M. Pecko, J. Mater. Sci. Lett. **19**, 1925 (2000)